

Communication

The Crystallization Process of Vaterite Microdisc Mesocrystals via Proto-Vaterite Amorphous Calcium Carbonate Characterized by Cryo-X-ray Absorption Spectroscopy

Li Qiao ¹, Ivo Zizak ², Paul Zaslansky ³ and Yurong Ma ^{1,*} 

¹ School of Chemistry and Chemical Engineering, Beijing Institute of Technology, Beijing 100081, China; qltrying@163.com

² Department Structure and Dynamics of Energy Materials, Helmholtz-Zentrum-Berlin, 14109 Berlin, Germany; zizak@helmholtz-berlin.de

³ Department for Operative and Preventive Dentistry, Charité-Universitätsmedizin Berlin, 10117 Berlin, Germany; paul.Zaslansky@charite.de

* Correspondence: yurong.ma@bit.edu.cn

Received: 27 July 2020; Accepted: 23 August 2020; Published: 26 August 2020



Abstract: Investigation on the formation mechanism of crystals via amorphous precursors has attracted a lot of interests in the last years. The formation mechanism of thermodynamically meta-stable vaterite in pure alcohols in the absence of any additive is less known. Herein, the crystallization process of vaterite microdisc mesocrystals via proto-vaterite amorphous calcium carbonate (ACC) in isopropanol was tracked by using Ca K-edge X-ray absorption spectroscopy (XAS) characterization under cryo-condition. Ca K-edge X-ray absorption near edge structure (XANES) spectra show that the absorption edges of the Ca ions of the vaterite samples with different crystallization times shift to lower photoelectron energy while increasing the crystallization times from 0.5 to 20 d, indicating the increase of crystallinity degree of calcium carbonate. Ca K-edge extended X-ray absorption fine structure (EXAFS) spectra exhibit that the coordination number of the nearest neighbor atom O around Ca increases slowly with the increase of crystallization time and tends to be stable as 4.3 (± 1.4). Crystallization time dependent XANES and EXAFS analyses indicate that short-range ordered structure in proto-vaterite ACC gradually transform to long-range ordered structure in vaterite microdisc mesocrystals via a non-classical crystallization mechanism.

Keywords: EXAFS; vaterite; proto-vaterite ACC; crystallization mechanism; isopropanol

1. Introduction

Calcium carbonate is one of the most abundant biominerals existing in nature, which is often applied as a crystallization model for the investigation of nucleation and crystal growth mechanism [1,2]. The polymorphs of calcium carbonate crystals include three anhydrous crystals: calcite [3], aragonite [4], and vaterite [5], and three hydrated crystal forms: calcium carbonate monohydrate, ikaite, and calcium carbonate hemihydrate [6]. In addition, there are a few amorphous calcium carbonate (ACC) phases with different water contents, which are important precursors in both biomineralization and bio-inspired crystallization systems [7–12]. Vaterite is the thermodynamically least stable phase of the three anhydrous crystalline phases. Different solvents and additives can induce the nucleation and crystallization of thermodynamically meta-stable vaterite. Vaterite crystals have been synthesized in aqueous solutions [13–15], alcohol–water mixed solvents [16,17], dimethyl formamide–water mixed

solvents [13,18], and non-aqueous solvents [19,20]. Vaterite crystals were successfully synthesized in the presence of additives such as proteins [21], peptides [22], amino acids [23], and polyalcohols [24].

Besides the classical theory of nucleation and crystallization based on atoms, ions and small molecules, non-classical nucleation and crystallization mechanism was proposed as a complementary novel crystallization mechanism which uses amorphous intermediate precursors such as droplets, clusters, or oligomers as intermediate phases or precursors of crystallization [25,26]. It is still a challenge to elucidate how intermediate precursors in solutions convert to different crystalline phases through multiple phase transformations [27]. A lot of studies have focused on the crystallization mechanisms by using anhydrous calcium carbonate forms such as calcite and aragonite as crystallization models while the formation of the thermodynamically least stable vaterite is less known. Solid state transformation from ACC to vaterite was observed by using Cryo-transmission electron microscopy (TEM) [28] and synchrotron-based in situ time-resolved energy dispersive X-ray diffraction (ED-XRD) [29] and X-ray absorption spectroscopy (XAS) [27,30].

XAS analysis provides high resolution structural information on the local atomic environment, the nearest neighbor shells around a metal ion of interest [31]. XAS has been applied to study the formation processes of biogenic and synthetic calcium carbonates [7,27,30,32]. XAS characterization of ACC deposited in crustacea *Porcellio scaber* showed short-range order which is comparable to crystalline calcium carbonate phases [32]. The local coordination environment of Ca ions in early structures involved in calcium carbonate mineral formation was studied by using conventional XAS [30]. Gebauer and coworkers applied XAS to distinguish synthetic additive-free proto-calcite ACC and proto-vaterite ACC which have different short-range ordered structures [7]. The intermediate phases involved during calcium carbonate crystallization from aqueous solutions were captured by using in situ XAS [27].

In our previous research, we reported the synthesis of vaterite microdisc mesocrystals exposing the (001) facet in isopropanol in the absence of any additive for the first time through a gas diffusion method [33]. It was proposed that vaterite microdisc mesocrystals are transformed via proto-vaterite ACC according to XAS analysis of the ACC precursor and well crystallized vaterite mesocrystals (vaterite obtained after crystallization for 10 days). In the work described herein, to investigate the crystallization mechanism of vaterite microdisc mesocrystals and the variation of the local atomic environment of Ca ions in calcium carbonate samples crystallized for different times, the formation process of vaterite microdisc mesocrystals via proto-vaterite ACC was tracked by using Ca K-edge XAS characterization under cryo-condition at 30 K. The absorption edges of the Ca ions of the vaterite samples shift to lower photoelectron energy according to the X-ray absorption near edge structure (XANES) spectra while increasing the crystallization times, indicating the increase of crystallinity of calcium carbonate. The coordination numbers of vaterite samples crystallized for different times generally increase from 3.4 (± 1.1) to 4.3 (± 1.4) with the increase of the crystallization time according to the fitting results of the Ca K-edge X-ray absorption fine structure (EXAFS) spectra for the first coordination shell (Ca-O₁).

2. Materials and Methods

2.1. Materials

Calcium chloride (CaCl₂·2H₂O, 99%) was purchased from Alfa Aesar. Analytical grade ammonium bicarbonate (NH₄HCO₃) was purchased from Yongda Chemical Reagent Co., China. Analytical grade isopropanol was purchased from Beijing Tongguang Fine Chemical Company. Analytical grade sulfuric acid was purchased from Xilong Chemical Co., China. All reagents were used without further purification.

2.2. Sample Synthesis

Vaterite microdisc mesocrystals were prepared by gas diffusion method. 0.25 g CaCl₂·2H₂O was dissolved into 40 mL of isopropanol under ultrasonication. The beaker containing the mixture

was covered with Parafilm punched with seven needle holes and then put in a desiccator. A beaker containing 4 g of NH_4HCO_3 was placed at the bottom of the desiccator as the source of CO_2 . A small bottle containing 20 mM H_2SO_4 was also placed in the desiccator to absorb the NH_3 gas. After 24 h of reaction time, the white suspension in the beaker was transferred into a sealed bottle and stood for different times for crystallization at ambient condition. The precipitated CaCO_3 particles in the bottle were isolated by centrifugation, washed twice with isopropanol and then dried in a vacuum oven overnight at room temperature [33].

2.3. X-ray Absorption Spectroscopy (XAS) Measurement

Crystallization time dependent XAS measurements were carried out using cyro-system at KMC-3 beamline in the Helmholtz Zentrum Berlin GmbH (HZB) [34], Germany. Ca K-edge information was collected in fluorescence mode under a liquid helium atmosphere at 30 K. The spot size of incident beam is $100 \times 100 \mu\text{m}^2$. Several scans were collected and combined together as one spectrum to improve the signal-to-noise ratio. The original data were processed and optimized by deglitching, energy calibration, alignment, merging, normalization, and self-absorption correction using ATHENA software. Fitting of the optimized data for every sample was performed using ARTEMIS software. For the fitting of all coordination shells of Ca ions in calcium carbonate, we gradually increased the scattering paths with the increase of the radius distance. There was a slight variation for the choice of R range and k range. For the fitting of the first coordination shell of Ca ions in calcium carbonate, the experimental data including the proto-ACC, the vaterite samples with different crystallization time and the vaterite reference were fitted as one combined data set. The R range was 1.25–2.5 Å, the k range was 3–9.5 Å⁻¹.

3. Results and Discussion

3.1. Ca K-Edge X-ray Absorption Near Edge Structure (XANES) Spectra

Proto-vaterite ACC was synthesized as a precursor using gas diffusion method, which was then crystallized for 0.5, 1, 2, 4, 10, and 20 d, respectively. To simplify description, we term the calcium carbonate samples with different crystallization times, e.g., vaterite-0.5d means the sample was crystallized for 0.5 d while it may still contain a certain amount of proto-vaterite ACC. Herein, freshly prepared calcium carbonate samples with short crystallization times (from 0.5 to 4 d) were immediately characterized using XAS, while calcium carbonate samples obtained after long crystallization times (10 and 20 d) were prepared in advance for XAS measurement. Ca K-edge X-ray absorption near edge structure (XANES) spectra of CaCl_2 , proto-vaterite ACC, samples crystallized for different times and vaterite reference were shown in Figure 1. XANES spectra of other well crystallized calcium carbonate samples, calcite and aragonite were also performed as references (Figure A1). XANES data for proto-vaterite ACC, sample crystallized for 10 d (vaterite-10d) and three well-crystalline reference crystals (calcite, aragonite, and vaterite) were shown in our previous work [33]. There are significant differences for the Ca K-edge XANES data of the three crystalline references of calcium carbonate, calcite, vaterite and aragonite, indicating that the local chemical environments around Ca ions of the different crystal phases are different from each other.

CaCl_2 , proto-vaterite ACC, samples with different crystallization times, and vaterite reference show very similar Ca K-edge XANES spectra. It is obvious that the Ca K-edge peaks of calcium carbonate samples are broader than the peak of CaCl_2 . The spectra of proto-vaterite ACC and the samples at the early crystallization stage (0.5, 1, and 2 d) with less crystallinity degree are very similar to that of vaterite, indicating that proto-vaterite ACC and the partially crystallized samples have short-range ordered structure similar to that of vaterite. A pre-edge feature at 4043 eV can be seen from the XANES spectra of all the samples with different crystallization times, which is attributed to $1s \rightarrow 3d$ transition [7], similar to proto-vaterite ACC and vaterite reference. The transition from s orbitals to d orbitals is dipole-forbidden, which are not appeared in centrosymmetric coordination environment

(calcite). The white line peak around 4053 eV is corresponding to the K-edge of Ca ions, which is due to $1s \rightarrow 4p$ transition [7]. A post edge feature appears at 4061 eV. The absorption edges of Ca of the samples with different crystallization times generally shift to low photoelectron energy, from 4052.90 to 4052.29 eV, while increasing the crystallization times from 0.5 to 20 d, indicating the increase of crystallinity degree of calcium carbonate [27]. In comparison, the absorption edge of vaterite reference is at 4051.5 eV.

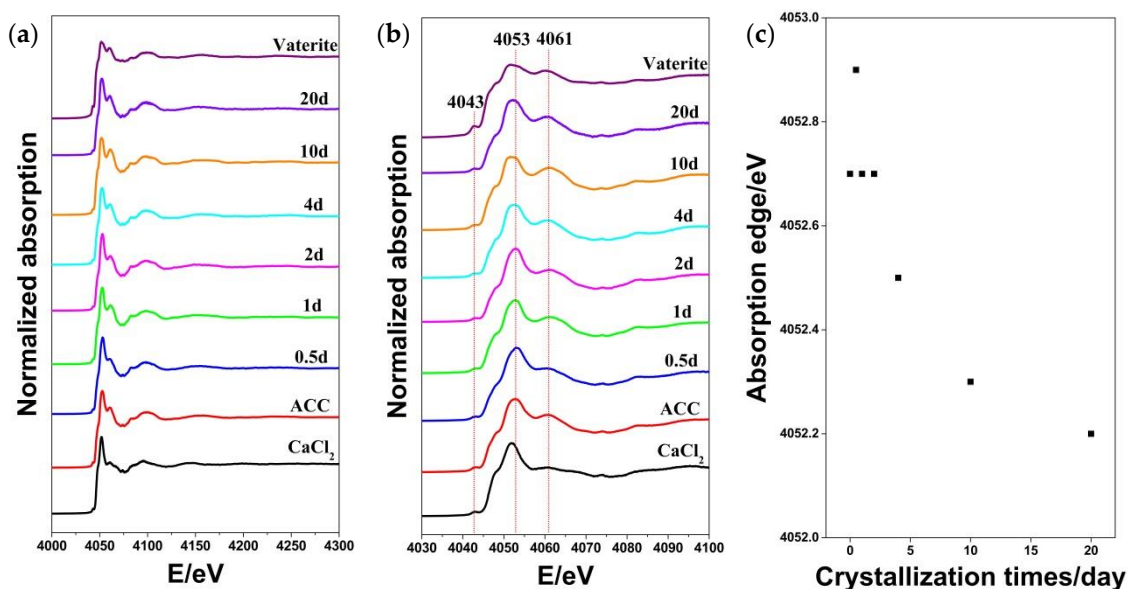


Figure 1. (a) Ca K-edge X-ray absorption near edge structure (XANES) spectra of CaCl₂, proto-vaterite, amorphous calcium carbonate (ACC), samples crystallized for different times and well-crystalline vaterite reference. (b) Magnified spectra for energy range between 4030 to 4100 eV. (c) The corresponding positions of the absorption edges of ACC and samples crystallized for different times. We marked the samples according to their crystallization times in the figures.

3.2. Ca K-Edge Extended X-ray Absorption Fine Structure (EXAFS) Spectra

Extended X-ray absorption fine structure (EXAFS) analysis was also proceeded in order to better understand the neighbor environment of the calcium ions, coordination number, and the distance of Ca to neighbor atoms. Ca K-edge extended X-ray absorption fine structure (EXAFS) spectra of proto-vaterite ACC, samples with different crystallization times and vaterite reference were plotted in R space (Fourier transform magnitude) and k space in Figure 2. The EXAFS spectra of proto-vaterite ACC, vaterite samples with different crystallization times and vaterite reference were fitted separately according to the lattice parameters and space group of vaterite (hexagonal $P3_221$) by using ARTEMIS, while FEFF was applied to calculate the EXAFS function for single scattering paths [35,36]. There are three energy-minimized structures having space groups $P6_5$, $P3_221$, and $P112_1$ [37] and it was noted that the $P3_221$ variant of this structure also fitted their XRD data well, and was calculated to be only ~ 1 kJ/mol different in energy from the $P6_522$ form [38]. The structures that have been proposed for vaterite are all based upon a common average structure with orientationally disordered carbonate groups [37]. The fitting results in R space of the four coordination shells of Ca ions including Ca-O₁ (the first coordination shell), Ca-C (the second coordination shell), Ca-O₂ (the third coordination shell), and Ca-Ca (the fourth coordination shell) are shown in Figure 2a, which are consistent very well with the experimental results when the R value is in between 2.0 and 3.5 Å. Considering that the proto-vaterite ACC precursors are composed of amorphous structures and don't own long-range order, only the first coordination shell close to the Ca ions, Ca-O₁, can be fitted well by using vaterite crystal as reference.

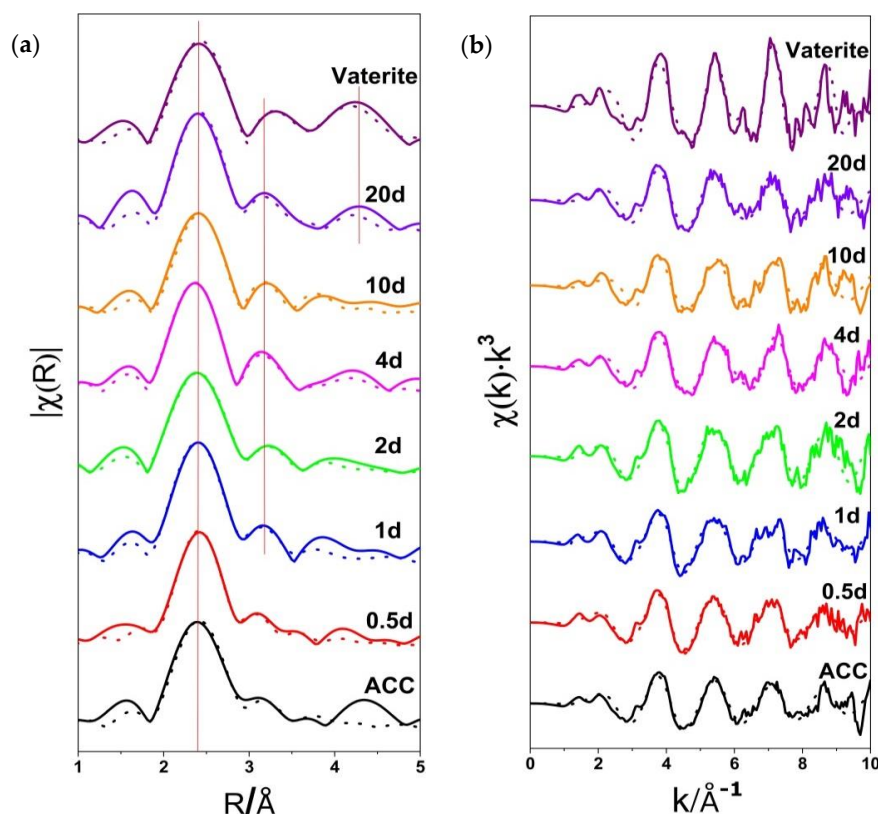


Figure 2. Ca K-edge extended X-ray absorption fine structure (EXAFS) spectra of experimental data (solid line) and the fitting results (dotted line) for proto-vaterite ACC and samples crystallized for different times and well-crystalline vaterite reference plotted in R space (Fourier transform magnitude) (a) and k space (b). The relative intensities of the $\chi(R)$ and $\chi(k)\cdot k^3$ were shown in Figure 2.

The peak for the first coordination shell (Ca-O_1) is strong in the EXAFS spectra (R space) of proto-vaterite ACC and vaterite-0.5d while the other peaks for the subsequent three coordination shells are barely distinguished. However, both the EXAFS spectra in R space of proto-vaterite ACC and vaterite-0.5d can be fitted well by using vaterite crystals, which indicates that short-range ordered atomic structure exists in the ACC and the very early crystallization stage (vaterite-0.5d). In comparison, the Ca K-edge EXAFS in R space of samples with crystallization times from 1 to 20 d show clearly a second peak, which are deduced to the second coordination shell (Ca-C) and the third coordination shell (Ca-O_2). The third peak, deduced to the fourth coordination shell (Ca-Ca), can be clearly distinguished while the crystallization time was extended to 20 d, which is similar to vaterite reference. The Ca K-edge EXAFS spectrum in R space of vaterite-20d is very similar to that of vaterite reference, indicating that the sample crystallized for 20 d has high crystallinity degree.

All the fitting results of Ca K-edge EXAFS in R space of proto-vaterite ACC and samples with different crystallization times from 0.5 to 20 d fit well with the experimental results. The R-factor values of the fittings are below 0.025, indicating relatively good fittings. Therefore, the proto-vaterite ACC and the partially crystallized samples at the early crystallization stage have the same short-range ordered structure with that of vaterite reference. The successive appearance of the second peak and the third peak in the Ca K-edge EXAFS spectra in R space with the extension of crystallization time indicates that the short-range ordered structures in the proto-vaterite ACC slowly transform to vaterite crystal with long-range ordered structure. In comparison, well crystallized calcite and aragonite show totally different EXAFS spectra in R space (Figure A2).

Figure 2b exhibited a k^3 -weighted $\chi(k)$ spectra of proto-vaterite ACC, samples with different crystallization times and vaterite reference. The Ca K-edge EXAFS spectrum in k space of proto-vaterite ACC looks like a modulated sinusoid, but the signals of well-crystallized vaterite crystals are less

sinusoidal. For well-crystalline vaterite crystals (vaterite reference, vaterite-20d), every Ca^{2+} ion and CO_3^{2-} ion are in a nearly identical environment apart from occasional defects and thermal vibrations [39]. The same local structures keep repeating. Finally, the signals of multiple ordered Ca ions are superimposed and show a non-sinusoidal spectrum. The higher order of the local atomic structures, the less sinusoidal shapes of the Ca K-edge EXAFS spectra in k space can be observed. The Ca K-edge EXAFS spectra in k space show a trend of less sinusoidal shape with the increase of crystallization time, which reveals that the ACC with short-range ordered structure is gradually replaced by crystalline structure with long-range ordered structure and the crystallinity degree of calcium carbonate increases while extending the crystallization time.

For the quantitative evaluation of the coordination environment, the EXAFS spectra of proto-vaterite ACC, vaterite samples with different crystallization times and vaterite reference were fitted as one combined data set while only the first coordination shell (Ca-O_1) was taken into account (Figure 3). Ca K-edge EXAFS spectra for the first coordination shell provides atomic distribution of the nearest-scattering atom, O, around Ca. The EXAFS spectra in k space of samples with different crystallization times exhibit obvious glitch peaks when the k value is bigger than 8 \AA^{-1} , illustrating that the data quality is poor at high k values ($>8 \text{ \AA}^{-1}$). Thus, we only fitted the first coordination shell to obtain more reliable coordination number of Ca ions.

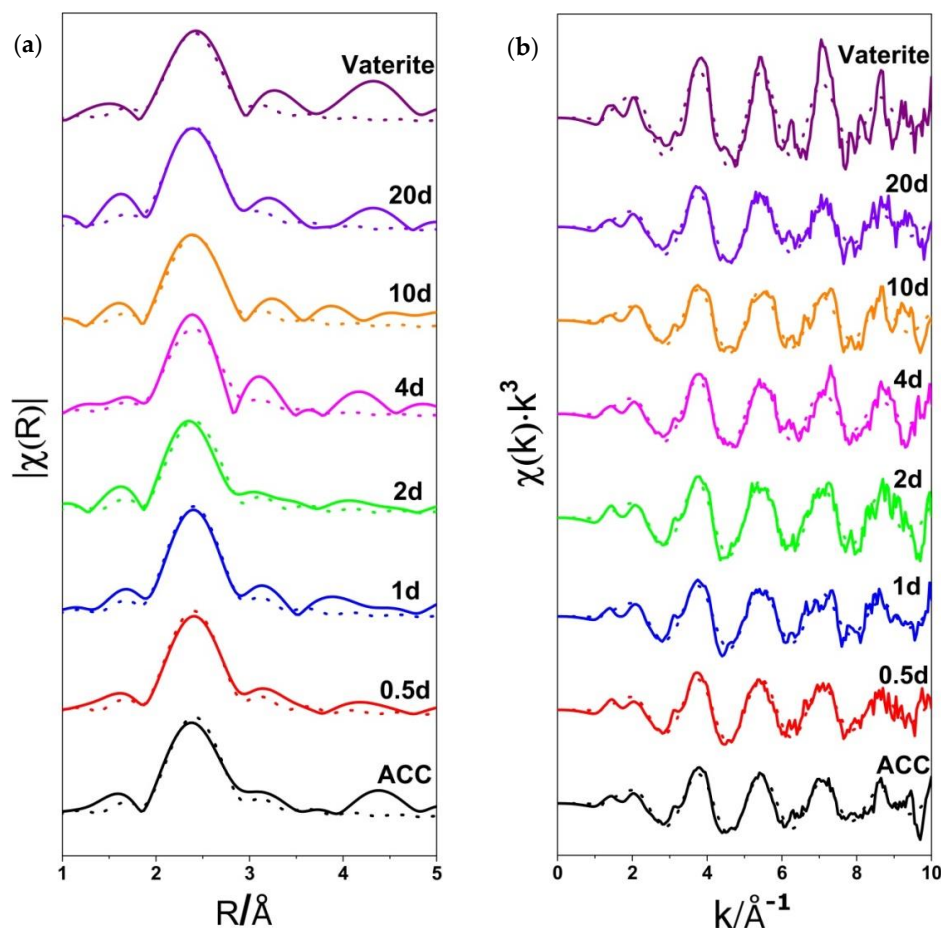


Figure 3. Ca K-edge extended X-ray absorption fine structure (EXAFS) spectra for the first coordination shell of the experimental data (solid line) and the fitting results (dotted line) for proto-vaterite ACC, samples crystallized for different times and well-crystalline vaterite reference plotted in R space (Fourier transform magnitude) (a) and k space (b).

The EXAFS amplitude (proportional to the coordination number) of proto-vaterite ACC and vaterite samples with different crystallization times were fitted as a portion of the EXAFS amplitude of

the vaterite reference, giving the relative occupation of the first shell, as compared to the reference sample. The distance of Ca and O of the first coordination shell (Ca-O₁) is $R_{\text{eff}} + \alpha R_{\text{ref}}$. The radial distances from Ca to O of the first coordination shell are the same for all samples due to using the combined fitting method and finally the fitting R value is 2.38 Å. The R-factor value of the fitting is 0.023. The Ca K-edge EXAFS spectra and the fitting results for the first coordination shell (Ca-O₁) are presented in Figure 3. The fitting results (N, the coordination number; R, the radial distance of the first coordination shell; σ^2 , the Debye-Waller factor) are summarized in Table 1.

Table 1. The first coordination shell (Ca-O₁) fitting results of proto-vaterite ACC, vaterite samples crystallized for different times and well-crystalline vaterite reference.

Sample	N	R(Å)	10 ³ σ ² (Å ²)
proto-vaterite ACC	3.5 (±0.8)		6 (±3)
vaterite-0.5d	3.4 (±1.1)		5 (±4)
vaterite-1d	3.5 (±0.9)		6 (±3)
vaterite-2d	3.7 (±1.1)	2.38 (±0.007)	3 (±4)
vaterite-4d	4.3 (±1.1)		8 (±3)
vaterite-10d	3.7 (±0.9)		6 (±3)
vaterite-20d	4.3 (±1.4)		8(±5)
vaterite reference	6 (±0)		6(±3)

The N of the samples at the early crystallization stages from 0.5 to 2 d increased from 3.4 (±1.1) to 3.7 (±1.1), very close to that of proto-vaterite ACC (3.5 (±0.8)). The N of vaterite-4d (4.3 (±1.1)) and vaterite-20d (4.3 (±1.4)) are obviously higher than those at early crystallization stages (0.5-2d), 3.4 to 3.7 (±1.1). Therefore, the coordination numbers of vaterite samples crystallized for different times generally increase from 3.4 (±1.1) to 4.3 (±1.4) with the increase of the crystallization time from 0.5 to 20 d, while the coordination number of vaterite reference is 6. The N of vaterite-10d is 3.7 (±0.9), lower than that of vaterite-4d (4.3 (±1.1)). We assume that the N value of vaterite-10d is not very precise. A possible reason is that the signal to noise ratio of the EXAFS spectrum of vaterite-10d is not very high, which might decrease the fitting quality. The Debye-Waller factor (σ^2) shows the mean square disorder of the distance to the neighboring atom [8]. The Debye-Waller factors of proto-vaterite ACC, vaterite samples with different crystallization times are all smaller than 0.01 Å² and similar to each other.

3.3. Discussion

Proto-vaterite ACC was successfully obtained in isopropanol by using a gas diffusion method. Despite the existence of short-range ordered structure in ACC can be confirmed according to characterization techniques such as XAS, solid state NMR [7], it remains a puzzle how the short-range ordered structures in ACC form [40]. According to our previous work, we proposed that proto-vaterite ACC nanoparticles aggregate in isopropanol and then vaterite nuclei form and start to grow via the condensation of proto-vaterite ACC nanoparticles and form vaterite microdisc mesocrystals [33], a typical mesocrystallization process [26,41]. The formation of proto-vaterite ACC instead of other kinds of ACC in isopropanol might be related to the stabilization of isopropanol for vaterite. And, the crystallinity degrees of vaterite samples increase with the increase of crystallization times according to the TEM, powder X-ray diffraction (PXRD), and fourier transform infrared spectroscopy (FTIR) results [33]. In this work, XAS characterizations for ACC and samples crystallized for different times were carried out under cryo-condition. Ultra-low temperature plays an important role in quenching crystallization of samples under irradiation of high energy X-ray beam, which limits the variation of structure phases. Therefore, cryo-XAS can exhibit the real structural information. XANES and EXAFS analyses in this article further show the gradual transformation from proto-vaterite ACC with short-range ordered structure to well crystallized vaterite with long-range ordered structure with the increase of crystallization times. XANES spectra show that the absorption edges of the Ca ions of the vaterite samples with different crystallization times shift from 4052.90 to 4052.29 eV while

increasing the crystallization times from 0.5 to 20 d, indicating the increase of crystallinity degree of calcium carbonate. EXAFS fitting results show that the coordination numbers of neighbor atom O around Ca in the first coordination shell increase from 3.4 (± 1.1) to 4.3 (± 1.4) with the increase of crystallization times from 0.5 to 20 d, which supports the above solid–solid transformation pathway. Instead of the first coordination shell (Ca-O₁), the peaks of the other three coordination shells (Ca-C, Ca-O₂, Ca-Ca) gradually appear with the increase of crystallization times. The short-range ordered structure in proto-vaterite ACC transform slowly to long-range ordered structure in vaterite. Then, the formed vaterite nanoparticles turn into vaterite microdisc mesocrystals through oriented attachment and secondary nucleation. It is suggested that both solid–solid transformation and dissolution and recrystallization exist simultaneously in crystallization process. Due to the low solubility of calcium carbonate in isopropanol, we propose that solid-solid transformation from proto-vaterite ACC to vaterite microdisc mesocrystals is the primary crystallization pathway, a mesocrystallization process, while dissolution and recrystallization are the minor pathways. The coordination number of O atoms in the first coordination shell for vaterite-20d (4.3 (± 1.4)) is lower than vaterite reference (6). A possible reason is that the interaction between OH[−] group and Ca²⁺ ions may result in a reduction in the fitted coordination number [7]. In addition, the multiple scattering paths may increase peak amplitudes. Ignoring multiple scattering could potentially lead to a slight underestimation of the amplitude of the EXAFS signal and thus the calculated coordination number is lower than the real systems [30].

4. Conclusions

The formation process of vaterite microdisc mesocrystals via proto-vaterite ACC was tracked by using Ca K-edge XAS characterization under cryo-condition at 30 K in this work. Ca K-edge XANES spectra show that the absorption edges of the Ca ions of the vaterite samples with different crystallization times shift to lower photoelectron energy while increasing the crystallization times, indicating the increase of crystallinity degree of calcium carbonate. Based on the fitting of the first coordination shell of the Ca K-edge EXAFS spectra, the coordination numbers of neighbor atom O around Ca for vaterite samples increase from 3.4 (± 1.1) to 4.3 (± 1.4) with the increase of crystallization times. Crystallization time dependent XANES and EXAFS analyses exhibited the variation of local coordination environment of Ca ions during the crystallization process, which show the gradual transformation from proto-vaterite ACC with short-range ordered structure to well crystallized vaterite with long-range ordered structure. XANES and EXAFS analyses show that the coordination environment of our samples becomes gradually ordered via ACC precursor during the crystallization process in isopropanol. According to the XAS analysis, it is proposed that both solid–solid transformation and dissolution and recrystallization exist simultaneously in crystallization process. XAS analysis under cryo-condition (cryo-XAS) can be applied as a very useful method to study the crystallization mechanism.

Author Contributions: Data collection, L.Q., P.Z., and I.Z.; writing—original draft preparation, L.Q.; writing—review and editing, Y.M.; supervision, Y.M.; project administration, Y.M.; funding acquisition, Y.M. All authors have read and agreed to the published version of the manuscript.

Funding: This research was funded by the National Key R&D Program of China (2018YFC1105100), National Natural Science Foundation of China (Grant No. 21877009), and Beijing Institute of Technology Research Fund Program for Young Scholars.

Acknowledgments: Thanks go to the HZB (Helmholtz-Zentrum Berlin) for allocation of beamtime and to Götz Schuck for help with the XAS measurements.

Conflicts of Interest: The authors declare no conflict of interest.

Appendix A

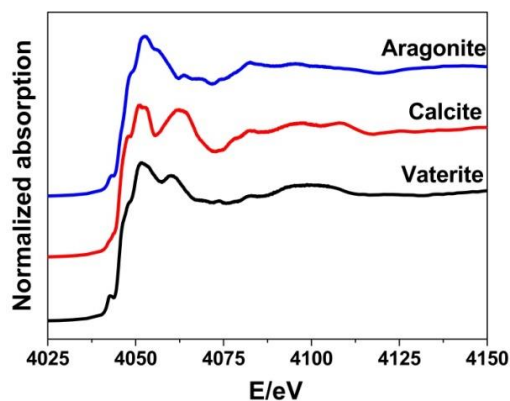


Figure A1. Ca K-edge X-ray absorption near edge structure (XANES) of three references, vaterite, calcite, aragonite.

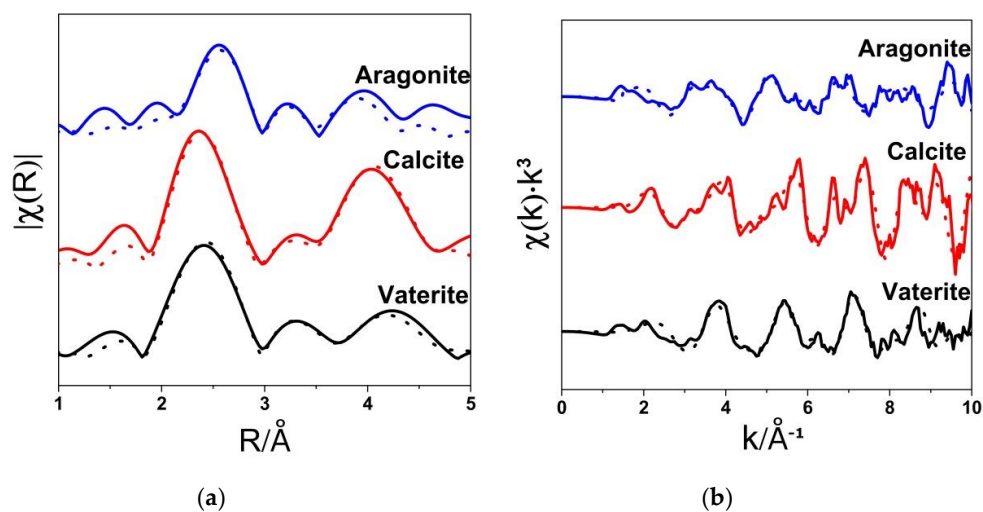


Figure A2. Ca K-edge extended X-ray absorption fine structure (EXAFS) spectroscopy of three references, vaterite, calcite, aragonite plotted in R space (Fourier transform magnitude) (a) and k space (b).

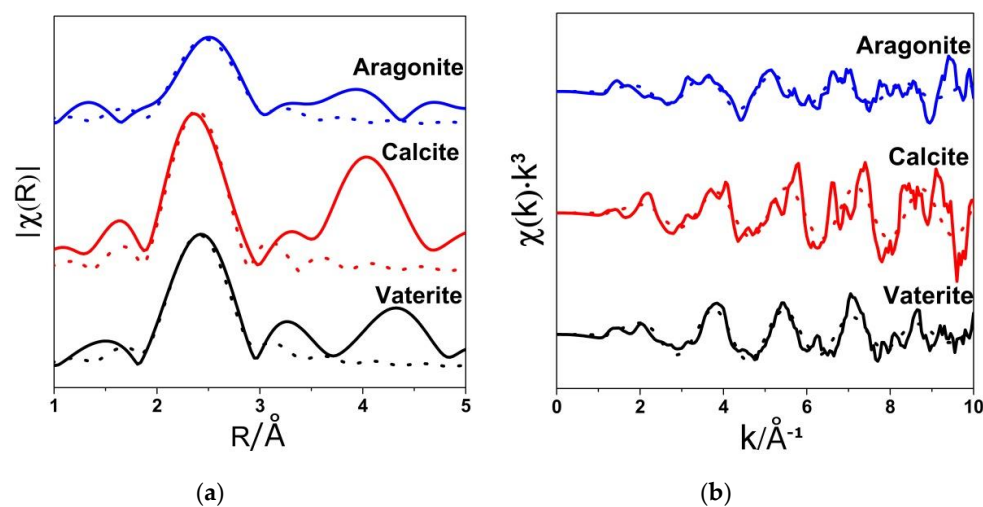


Figure A3. Ca K-edge extended X-ray absorption fine structure (EXAFS) spectra for the first coordination shell of three references, vaterite, calcite, aragonite plotted in R space (Fourier transform magnitude) (a) and k space (b).

Table A1. The first coordination shell (Ca-O₁) fitting results of three references, vaterite, calcite, aragonite.

Sample	N	R(Å)	10 ³ σ ² (Å ²)
Vaterite	6	2.38	6
Calcite	6	2.35	0.3
Aragonite	9	2.47	0.9

References

- Sommerdijk, N.A.J.M.; de With, G. Biomimetic CaCO₃ Mineralization using Designer Molecules and Interfaces. *Chem. Rev.* **2008**, *108*, 4499–4550. [[CrossRef](#)] [[PubMed](#)]
- Koishi, A.; Fernandez-Martinez, A.; Van Driessche, A.E.S.; Michot, L.J.; Pina, C.M.; Pimentel, C.; Lee, B.; Montes-Hernandez, G. Surface Wetting Controls Calcium Carbonate Crystallization Kinetics. *Chem. Mater.* **2019**, *31*, 3340–3348. [[CrossRef](#)]
- Falini, G.; Albeck, S.; Weiner, S.; Addadi, L. Control of aragonite or calcite polymorphism by mollusk shell macromolecules. *Science* **1996**, *271*, 67–69. [[CrossRef](#)]
- Nemeth, P.; Mugnaioli, E.; Gemmi, M.; Czuppon, G.; Demeny, A.; Spotl, C. A nanocrystalline monoclinic CaCO₃ precursor of metastable aragonite. *Sci. Adv.* **2018**, *4*, 6178–6190. [[CrossRef](#)] [[PubMed](#)]
- Kabalah-Amitai, L.; Mayzel, B.; Kauffmann, Y.; Fitch, A.N.; Bloch, L.; Gilbert, P.U.P.A.; Pokroy, B. Vaterite Crystals Contain Two Interspersed Crystal Structures. *Science* **2013**, *340*, 454–457. [[CrossRef](#)]
- Zou, Z.Y.; Habraken, W.J.E.M.; Matveeva, G.; Jensen, A.C.S.; Bertinetti, L.; Hood, M.A.; Sun, C.Y.; Gilbert, P.U.P.A.; Polishchuk, I.; Pokroy, B.; et al. A hydrated crystalline calcium carbonate phase: Calcium carbonate hemihydrate. *Science* **2019**, *363*, 396–400. [[CrossRef](#)]
- Gebauer, D.; Gunawidjaja, P.N.; Ko, J.Y.; Bacsik, Z.; Aziz, B.; Liu, L.; Hu, Y.; Bergstrom, L.; Tai, C.W.; Sham, T.K.; et al. Proto-calcite and proto-vaterite in amorphous calcium carbonates. *Angew. Chem. Int. Ed.* **2010**, *49*, 8889–8891. [[CrossRef](#)]
- Du, H.; Steinacher, M.; Borca, C.; Huthwelker, T.; Murello, A.; Stellacci, F.; Amstad, E. Amorphous CaCO₃: Influence of the Formation Time on Its Degree of Hydration and Stability. *J. Am. Chem. Soc.* **2018**, *140*, 14289–14299. [[CrossRef](#)]
- DeVol, R.T.; Sun, C.Y.; Marcus, M.A.; Coppersmith, S.N.; Myneni, S.C.B.; Gilbert, P.U.P.A. Nanoscale Transforming Mineral Phases in Fresh Nacre. *J. Am. Chem. Soc.* **2015**, *137*, 13325–13333. [[CrossRef](#)]
- Farhadi-Khouzani, M.; Chevrier, D.M.; Zhang, P.; Hedin, N.; Gebauer, D. Water as the Key to Proto-Aragonite Amorphous CaCO₃. *Angew. Chem. Int. Ed.* **2016**, *55*, 8117–8120. [[CrossRef](#)]
- Walker, J.M.; Marzec, B.; Nudelman, F. Solid-State Transformation of Amorphous Calcium Carbonate to Aragonite Captured by CryoTEM. *Angew. Chem. Int. Ed.* **2017**, *56*, 11740–11743. [[CrossRef](#)] [[PubMed](#)]
- Levi-Kalisman, Y.; Raz, S.; Weiner, S.; Addadi, L.; Sagi, I. Structural differences between biogenic amorphous calcium carbonate phases using X-ray absorption spectroscopy. *Adv. Funct. Mater.* **2002**, *12*, 43–48. [[CrossRef](#)]
- Zhang, J.; Li, Y.; Xie, H.; Su, B.L.; Yao, B.; Yin, Y.X.; Li, S.P.; Chen, F.; Fu, Z.Y. Calcium Carbonate Nanoplate Assemblies with Directed High-Energy Facets: Additive-Free Synthesis, High Drug Loading, and Sustainable Releasing. *ACS Appl. Mater. Interfaces* **2015**, *7*, 15686–15691. [[CrossRef](#)] [[PubMed](#)]
- Schenk, A.S.; Cantaert, B.; Kim, Y.Y.; Li, Y.T.; Read, E.S.; Semsarilar, M.; Armes, S.P.; Meldrum, F.C. Systematic Study of the Effects of Polyamines on Calcium Carbonate Precipitation. *Chem. Mater.* **2014**, *26*, 2703–2711. [[CrossRef](#)]
- Li, X.Q.; Zeng, H.C. Calcium Carbonate Nanotablets: Bridging Artificial to Natural Nacre. *Adv. Mater.* **2012**, *24*, 6277–6282. [[CrossRef](#)]
- Imai, H.; Tochimoto, N.; Nishino, Y.; Takezawa, Y.; Oaki, Y. Oriented Nanocrystal Mosaic in Monodispersed CaCO₃ Microspheres with Functional Organic Molecules. *Cryst. Growth Des.* **2012**, *12*, 876–882. [[CrossRef](#)]
- Sand, K.K.; Rodriguez-Blanco, J.D.; Makovicky, E.; Benning, L.G.; Stipp, S.L.S. Crystallization of CaCO₃ in Water-Alcohol Mixtures: Spherulitic Growth, Polymorph Stabilization, and Morphology Change. *Cryst. Growth Des.* **2012**, *12*, 842–853. [[CrossRef](#)]
- Zhang, J.; Yao, B.; Ping, H.; Fu, Z.Y.; Li, Y.; Wang, W.M.; Wang, H.; Wang, Y.C.; Zhang, J.Y.; Zhang, F. Template-free synthesis of hierarchical porous calcium carbonate microspheres for efficient water treatment. *RSC Adv.* **2016**, *6*, 472–480. [[CrossRef](#)]

19. Sun, R.; Willhammar, T.; Grape, E.S.; Stromme, M.; Cheung, O. Mesoscale Transformation of Amorphous Calcium Carbonate to Porous Vaterite Microparticles with Morphology Control. *Cryst. Growth Des.* **2019**, *19*, 5075–5087. [[CrossRef](#)]
20. Magnabosco, G.; Polishchuk, I.; Pokroy, B.; Rosenberg, R.; Cölfen, H.; Falini, G. Synthesis of calcium carbonate in trace water environments. *Chem. Commun.* **2017**, *53*, 4811–4814. [[CrossRef](#)]
21. Rugabirwa, B.; Murindababisha, D.; Wang, H.T.; Li, J. A High-Pressure Gas Solid Carbonation Route to Produce Vaterite. *Cryst. Growth Des.* **2019**, *19*, 242–248. [[CrossRef](#)]
22. Lu, H.; Lutz, H.; Roeters, S.J.; Hood, M.A.; Schafer, A.; Munoz-Espi, R.; Berger, R.; Bonn, M.; Weidner, T. Calcium-Induced Molecular Rearrangement of Peptide Folds Enables Biomineralization of Vaterite Calcium Carbonate. *J. Am. Chem. Soc.* **2018**, *140*, 2793–2796. [[CrossRef](#)] [[PubMed](#)]
23. Jiang, W.; Pacella, M.S.; Athanasiadou, D.; Nelea, V.; Vali, H.; Hazen, R.M.; Gray, J.J.; McKee, M.D. Chiral acidic amino acids induce chiral hierarchical structure in calcium carbonate. *Nat. Commun.* **2017**, *8*, 15066. [[CrossRef](#)] [[PubMed](#)]
24. Svenskaya, Y.I.; Fattah, H.; Inozemtseva, O.A.; Ivanova, A.G.; Shtykov, S.N.; Gorin, D.A.; Parakhonskiy, B.V. Key Parameters for Size- and Shape-Controlled Synthesis of Vaterite Particles. *Cryst. Growth Des.* **2018**, *18*, 331–337. [[CrossRef](#)]
25. Niederberger, M.; Cölfen, H. Oriented attachment and mesocrystals: Non-classical crystallization mechanisms based on nanoparticle assembly. *Phys. Chem. Chem. Phys.* **2006**, *8*, 3271–3287. [[CrossRef](#)]
26. Jehannin, M.; Rao, A.; Cölfen, H. New Horizons of Nonclassical Crystallization. *J. Am. Chem. Soc.* **2019**, *141*, 10120–10136. [[CrossRef](#)]
27. Xto, J.; Wetter, R.; Borca, C.N.; Frieh, C.; van Bokhoven, J.A.; Huthwelker, T. Droplet-based in situ X-ray absorption spectroscopy cell for studying crystallization processes at the tender X-ray energy range. *RSC Adv.* **2019**, *9*, 34004–34010. [[CrossRef](#)]
28. Pouget, E.M.; Bomans, P.H.H.; Dey, A.; Frederik, P.M.; de With, G.; Sommerdijk, N.A.J.M. The Development of Morphology and Structure in Hexagonal Vaterite. *J. Am. Chem. Soc.* **2010**, *132*, 11560–11565. [[CrossRef](#)]
29. Rodriguez-Blanco, J.D.; Shaw, S.; Benning, L.G. The kinetics and mechanisms of amorphous calcium carbonate (ACC) crystallization to calcite, via vaterite. *Nanoscale* **2011**, *3*, 265–271. [[CrossRef](#)]
30. Avaro, J.; Moon, E.M.; Rose, J.; Rose, A.L. Calcium coordination environment in precursor species to calcium carbonate mineral formation. *Geochim. Cosmochim. Acta* **2019**, *259*, 344–357. [[CrossRef](#)]
31. Koningsberger, D.C.; Prins, R. (Eds.) *X-ray Absorption: Principles, Applications and Techniques of EXAFS, SEXAFS and XANES*; Wiley: New York, NY, USA, 1988; Volume 1.
32. Becker, A.; Bismayer, U.; Epple, M.; Fabritius, H.; Hasse, B.; Shi, J.; Ziegler, A. Structural characterisation of X-ray amorphous calcium carbonate (ACC) in sternal deposits of the crustacea *Porcellio scaber*. *Dalton Trans.* **2003**, 551–555. [[CrossRef](#)]
33. Zhang, Y.Z.; Qiao, L.; Yan, H.J.; Zizak, I.; Zaslansky, P.; Li, Y.F.; Qi, L.M.; Ma, Y.R. Vaterite microdisc mesocrystals exposing the (001) facet formed via transformation from proto-vaterite amorphous calcium carbonate. *Cryst. Growth Des.* **2020**, *20*, 3482–3492. [[CrossRef](#)]
34. Görlin, M.; Chernev, P.; Ferreira de Araújo, J.; Reier, T.; Dresch, S.; Paul, B.; Krähnert, R.; Dau, H.; Strasser, P. Oxygen Evolution Reaction Dynamics, Faradaic Charge Efficiency, and the Active Metal Redox States of Ni-Fe Oxide Water Splitting Electrocatalysts. *J. Am. Chem. Soc.* **2016**, *138*, 5603–5614. [[CrossRef](#)] [[PubMed](#)]
35. Newville, M. IFEFFIT: Interactive XAFS analysis and FEFF fitting. *J. Synchrotron Rad.* **2001**, *8*, 322–324. [[CrossRef](#)] [[PubMed](#)]
36. Rehr, J.J.; Deleon, J.M.; Zabinsky, S.I.; Albers, R.C. Theoretical X-Ray Absorption Fine-Structure Standards. *J. Am. Chem. Soc.* **1991**, *113*, 5135–5140. [[CrossRef](#)]
37. Christy, A.G. A Review of the Structures of Vaterite: The Impossible, the Possible, and the Likely. *Cryst. Growth Des.* **2017**, *17*, 3567–3578. [[CrossRef](#)]
38. Wang, J.W.; Zhang, F.X.; Zhang, J.M.; Ewing, R.C.; Becker, U.; Cai, Z.H. Carbonate orientational order and superlattice structure in vaterite. *J. Cryst. Growth* **2014**, *407*, 78–86. [[CrossRef](#)]
39. Calvin, S. XAFS in a Nutshell. In *XAFS for Everyone*; CRC Press: Boca Raton, FL, USA, 2012; pp. 20–21.

40. Sun, S.; Chevrier, D.M.; Zhang, P.; Gebauer, D.; Cölfen, H. Distinct Short-Range Order Is Inherent to Small Amorphous Calcium Carbonate Clusters (<2 nm). *Angew. Chem. Int. Ed.* **2016**, *55*, 12206–12209.
41. Gebauer, D.; Cölfen, H. Prenucleation clusters and non-classical nucleation. *Nano Today* **2011**, *6*, 564–584. [[CrossRef](#)]



© 2020 by the authors. Licensee MDPI, Basel, Switzerland. This article is an open access article distributed under the terms and conditions of the Creative Commons Attribution (CC BY) license (<http://creativecommons.org/licenses/by/4.0/>).